

## Supporting Information

### **Ultrathin iridium carbonyl formate for efficient and durable acidic oxygen evolution electrocatalysis**

Jian Wei Guo,<sup>#a</sup> Fangxin Mao,<sup>#a</sup> Song Ru Fang,<sup>a</sup> Hao Yang Lin,<sup>a</sup> Huan Wang,<sup>a</sup> Wen  
Jing Li,<sup>a</sup> Hai Yang Yuan,<sup>a</sup> Shuang Yang,<sup>\*a</sup> Peng Fei Liu<sup>\*a</sup> and Hua Gui Yang<sup>a</sup>

## Experimental Section

**Materials.** Iridium chloride hydrate ( $\text{IrCl}_3 \cdot x\text{H}_2\text{O}$ , metals basis, Ir > 52%) was purchased from Aladdin Scientific Corp and was dissolved in the ultrapure water to a concentration of  $10 \text{ mg mL}^{-1}$  for the further use. 1,3,5-benzenetricarboxylic acid (BTC, 98%) was purchased from J&K Scientific Co., Ltd. Perchloric acid ( $\text{HClO}_4$ , analysis reagent, 72%), N, N-Dimethylformamide (DMF, reagent grade, 99.8%) and formic acid (reagent grade, 98%) were provided by the Sinopharm Chemical Reagent Co., Ltd. Ethanol anhydrous (reagent grade, 99.7%) was purchased from the Lingfeng Chemical Reagent Co. Commercial Pt/C (40%), iridium black and iridium oxides nanomaterials were obtained from Shanghai Hesen Electric Co., Ltd. Nafion 115 was used as proton exchange membrane in the electrolyzer test.

**Sample preparation.** Microwave synthesis was adopted to prepare catalytic materials on the XH-300UL+ device equipped with a temperature-controlled unit. For IrCF-BTC sample synthesis, 3.5 mL  $\text{IrCl}_3$  aqueous solution was mixed with 5 mL DMF and 5 mL formic acid, and 7 mg BTC was then dissolved by ultrasonic. The mixture solution was transferred into microwave synthesis device and heated to  $100 \text{ }^\circ\text{C}$  in 5 min, following reaction for several minutes. The sample was collected after cooling by high-speed centrifugation with 10000 rpm for 10 min, using water and ethanol to wash the residual solvents. The additive amounts of BTC were 0 mg and 70 mg for samples of IrCF and IrCF-10BTC, correspondingly. IrCF-hydrothermal sample was prepared by heating the precursor of IrCF in a baking oven at  $80 \text{ }^\circ\text{C}$  for 12 h instead of microwave synthesis. All the samples were dried in a vacuum oven at  $80 \text{ }^\circ\text{C}$ .

**Characterizations.** The crystal structure was analyzed by X-ray diffraction (XRD, D8 ADVANCE, BRUKER) equipped with the Cu k radiation source, operating at voltage of

40 kV and current density of 40 mA. Fourier Transform - Infrared Spectrometer (FT-IR, Nicolet 7000-C) was operated to probe the function group in materials. The morphology was observed by the scanning electron microscopy (SEM, Hitachi S-4800) and aberration-corrected scanning transmission electron microscopy (STEM, Thermo Fisher Themis Z microscope) with accelerating voltage of 300 kV. Thermogravimetric analysis (TGA) was conducted on a Perkin-Elmer thermogravimetric analyzer with air atmosphere. Element analysis (EA) was tested on the equipment of vario EL cube (Elementar, Germany). X-ray absorption fine structure (XAFS) spectra were collected at the BL14W1 station in Shanghai Synchrotron Radiation Facility (SSRF), China. For iridium element, the L3-edge (11215 eV) was selected as absorption edge for measurement, in which Ir foil and commercial IrO<sub>2</sub> were as reference samples of metallic and oxidation states.

**Electrochemical measurements.** Three-electrode system and proton exchange membrane (PEM) electrolyzer device were used to estimate materials' performance of the acidic oxygen evolution catalysis. In three electrode system, electrolyte was 0.1 M HClO<sub>4</sub> solution. The catalysts were loaded onto glass carbon (diameter 3 mm) to form a working electrode. Catalysts ink contained 5 mg samples, 25  $\mu$ L Nafion (5 vol.%), and 475  $\mu$ L ethanol, which was prepared by ultrasonic. 4  $\mu$ L ink was drop-coated onto glass carbon electrode, drying naturally under ambient conditions. A Pt mesh with size of 1 cm  $\times$  1 cm and Ag/AgCl (packing with 3.5 M KCl solution) were used as the counter electrode and reference electrode, respectively. Measurements were operated on an electrochemical workstation of CHI 660e. Linear sweep voltammetry (LSV) was performed with a scanning rate of 5 mV s<sup>-1</sup> to determine the overpotential of water oxidation reaction. Electrochemical impedance spectroscopy (EIS) was performed with frequency range from 0.01 Hz to 10<sup>5</sup> Hz.

**PEMWE assembly and test.** For PEMWE device test, membrane electrode assemblies (MEAs) were fabricated with Pt/C (40 wt.%) cathodic materials and target anodic samples by hot-press method. Pt/C materials were air-sprayed onto Nafion 115 membrane with a loading of about  $1 \text{ mg cm}^{-2}$  before hot-pressing. The anodic catalyst samples were air-sprayed onto PTEF film with about  $1.4 \text{ mg cm}^{-2}$  loading mass, and transferred onto proton exchange membrane in the pressing procedure, leading to a three-layer MEA. Two porous transport layer (PTL) was covered on the catalyst layers of MEAs, and a five-layer MEAs were formed after clamping between the two Ti plate current collectors equipped with the serpentine flow channel. Pure water was heated to  $80 \text{ }^\circ\text{C}$  to feed anodic reagent by a thermostat water bath and a peristaltic pump. The polarization curves were collected from  $0.1 \text{ A cm}^{-2}$  to  $1.5 \text{ A cm}^{-2}$ . The stability of the PEM electrolyzers were evaluated by measuring chronopotentiometry at  $1.0 \text{ A cm}^{-2}$ .

**DFT calculation method.** All the spin-polarized DFT computations were performed by using the Vienna Ab initio simulation package (VASP)<sup>S1</sup> and the ion cores represented by the projector augmented wave (PAW) potentials. The generalized gradient approximation (GGA) in the form of the Perdew–Burke–Ernzerhof (PBE) functional was used in this work.<sup>S2</sup> A cutoff energy of 450 eV for the plane-wave basis set were adopted. The convergence threshold for the structure relaxation was set to be  $0.05 \text{ eV}\cdot\text{\AA}^{-1}$  in force and  $10^{-5} \text{ eV}$  in energy, respectively. A vacuum space exceeding  $15 \text{ \AA}$  was employed. The  $2 \times 2 \times 1$  Monkhorst–Pack k-point mesh was performed for all the calculation models. The van der Waals (vdW) interactions were taken into consideration using method of Grimme (DFT-D3).<sup>S3</sup>

The adsorption energy ( $E_{\text{ads}}$ ) can be calculated using the following equation:

$$\Delta E_{\text{ads}} = E_{\text{ads/slab}} - E_{\text{ads}} - E_{\text{slab}}$$

where  $E_{\text{ads/slab}}$ ,  $E_{\text{ads}}$  and  $E_{\text{slab}}$  are the total energies for adsorbed species on slab, adsorbed species and isolated slab, respectively.

The free energy of a proton/electron pair ( $\text{H}^+ + \text{e}^-$ ) is equal to half of the gaseous hydrogen ( $1/2\text{H}_2$ ) at an equilibrium potential for each process, namely the free energy variations for each process were calculated based on computational hydrogen electrode (CHE) model.

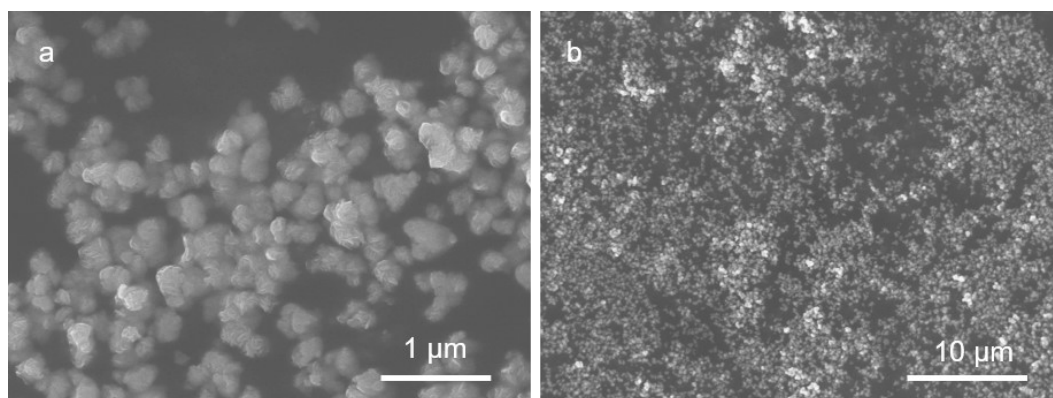


**Fig. S1.** (a) and (b) SEM images of IrCF-BTC samples at different magnifications.

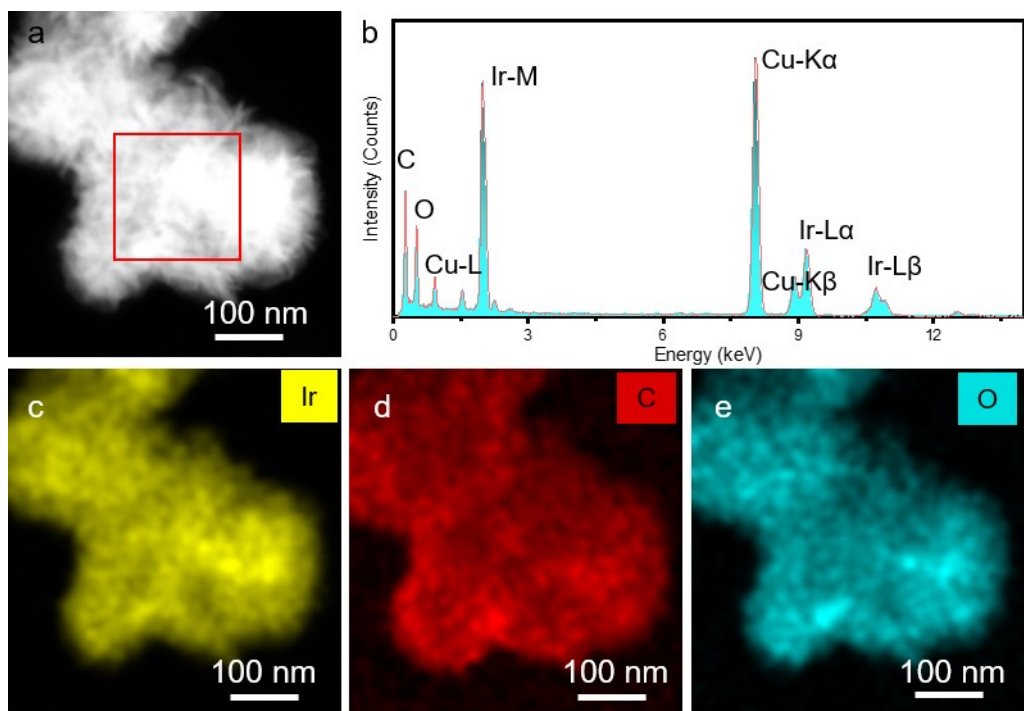


**Fig. S2.** (a) HAADF-STEM image of IrCF-BTC sample for energy dispersive spectroscopy analysis. (b) EDS spectrum of IrCF-BTC for the selected area in (a). (c-e) Element maps of Ir, C, and O based on the surface scanning results, revealing the uniform distribution of elements in the sample.

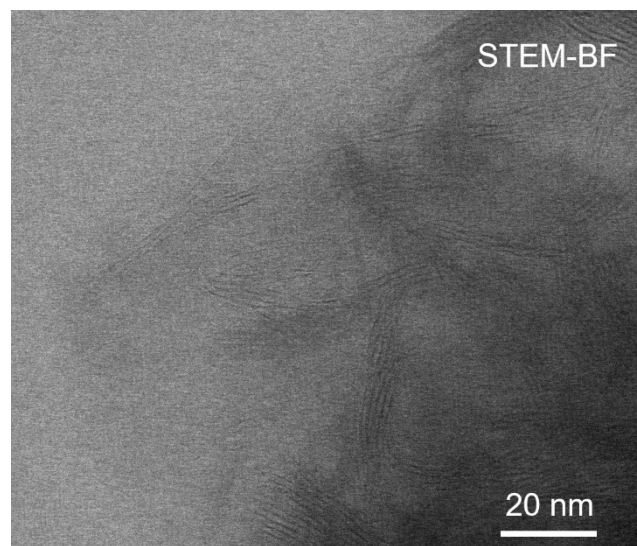


**Fig. S3.** Bright field (BF)-STEM image of IrCF-BTC sample, in which ultrathin stacked flakes could be observed.

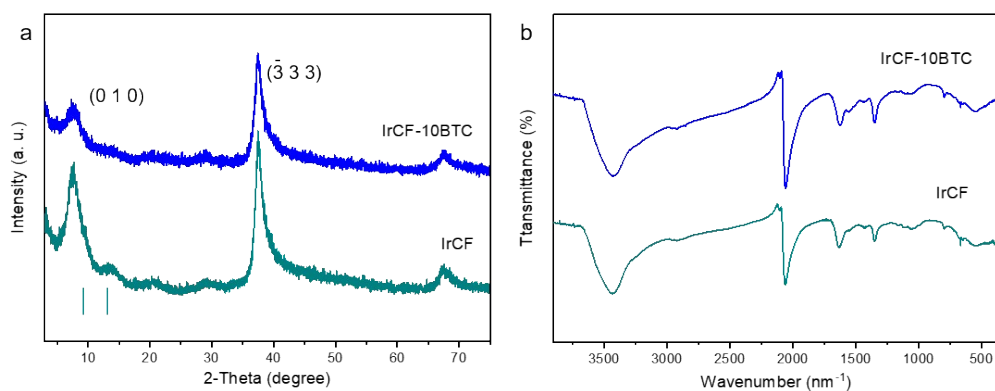


**Fig. S4.** (a) XRD patterns and (b) FTIR spectra of IrCF and IrCF-10BTC samples. Similar crystal structure could be demonstrated for samples with and without BTC regulators.

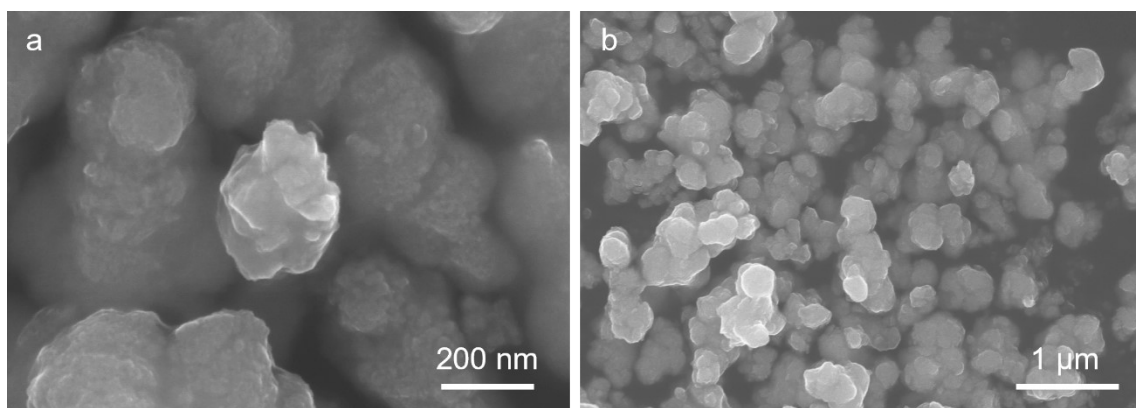


**Fig. S5.** (a, b) SEM images of IrCF-hydrothermal sample with the nanoparticles structure.

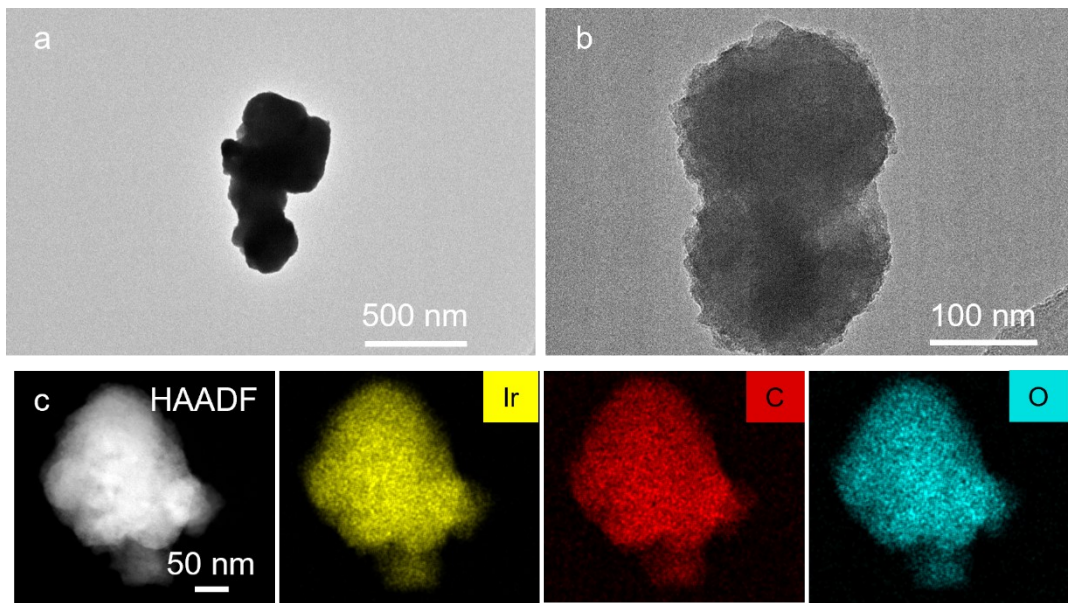


**Fig. S6.** TEM characterizations of IrCF-hydrothermal sample. (a) Low magnification image. (b) High magnification image. (c) Element mapping images of Ir, C, and O in IrCF-hydrothermal.

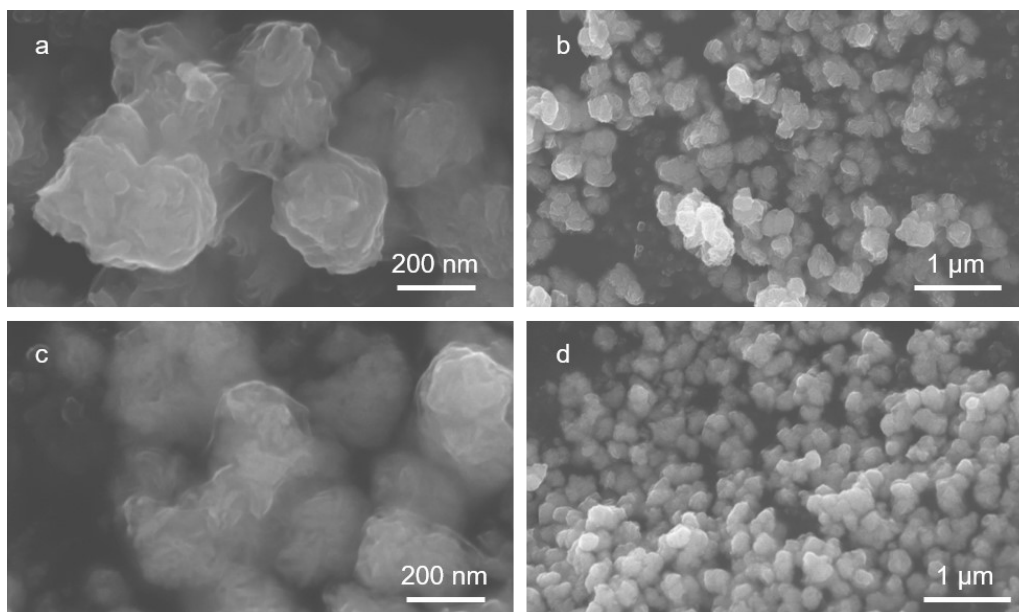


**Fig. S7.** (a, b) SEM images of IrCF sample with absence of BTC ligands in synthesis. (c, d) SEM images of IrCF-10BTC with more addition of BTC regulators.

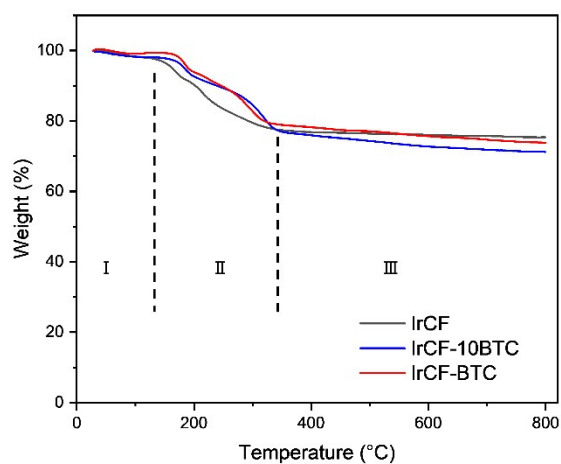


**Fig. S8.** TGA curves of IrCF, IrCF-BTC, and IrCF-10BTC samples under air atmosphere.

**Table S1.** Component test result of the samples based on element analysis equipment.

Sample\Element	H [wt.%]	C [wt.%]	O [wt.%]
IrCF	0.746	9.980	14.375
IrCF-BTC	0.747	9.960	13.943
IrCF-10BTC	0.601	8.570	14.229

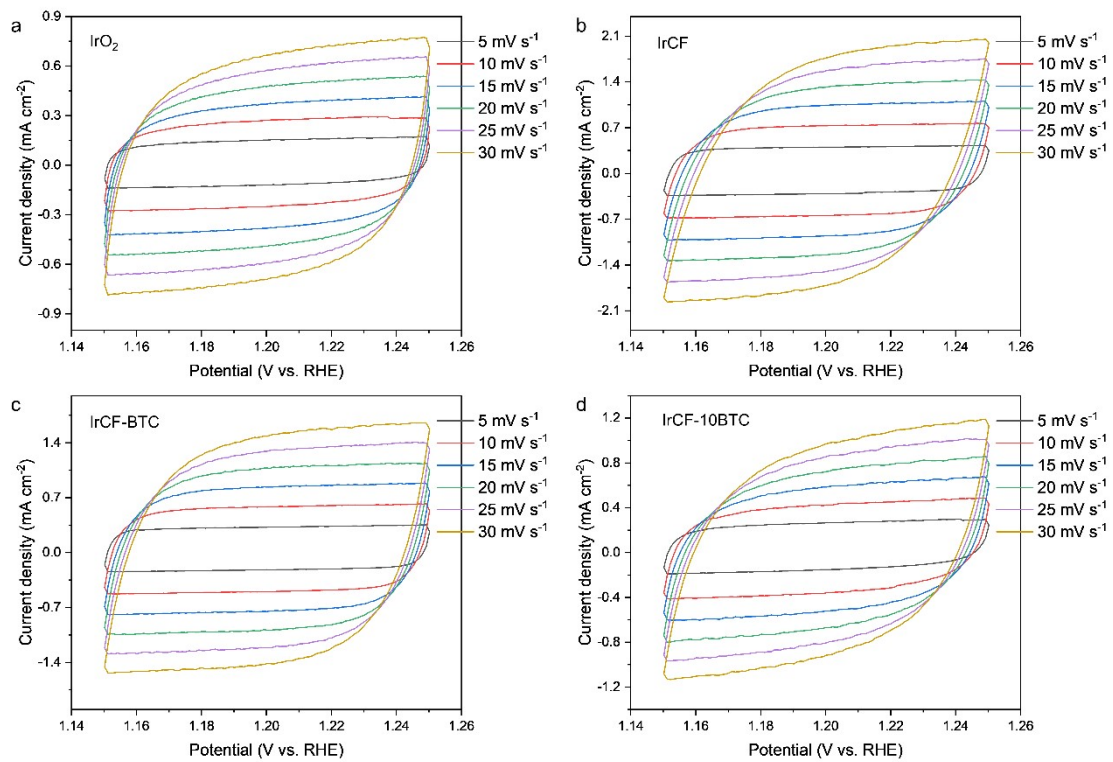


**Fig. S9.** Cyclic voltammetry curves of commercial IrO<sub>2</sub>, as-prepared IrCF, IrCF-BTC, and IrCF-10BTC samples at the varied scan rates.

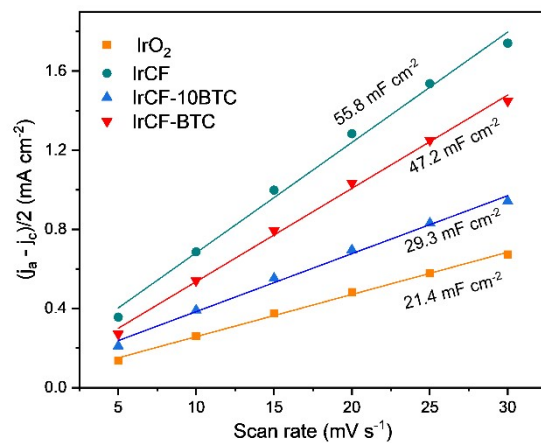


**Fig. S10.** Electric double-layer capacitances obtained by fitting the non-faradaic current and scan rates from the CV results.

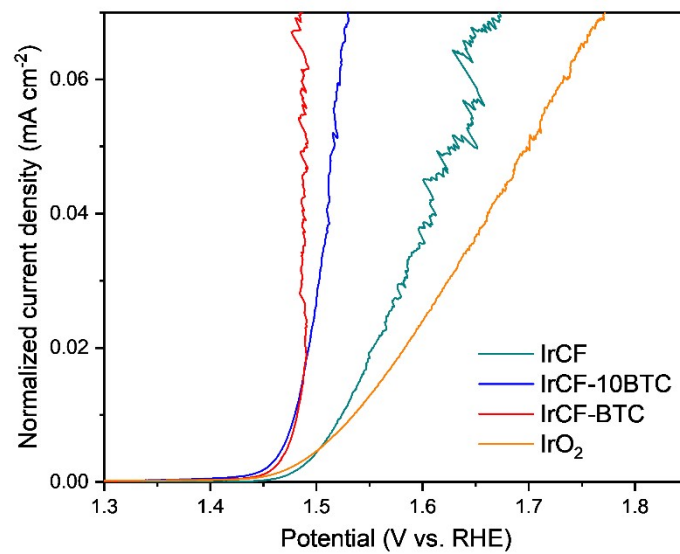


**Fig. S11.** Normalized LSV curves by the calculated ECSA based on the IrO<sub>2</sub>.

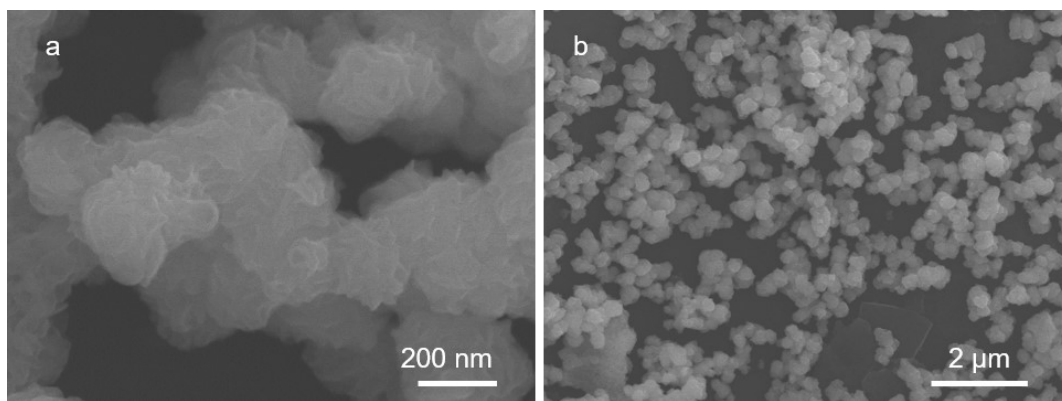


**Fig. S12.** (a, b) SEM images of IrCF-BTC samples after long term electrolysis at a current density of  $10 \text{ mA cm}^{-2}$  in  $0.1 \text{ M HClO}_4$  solution.

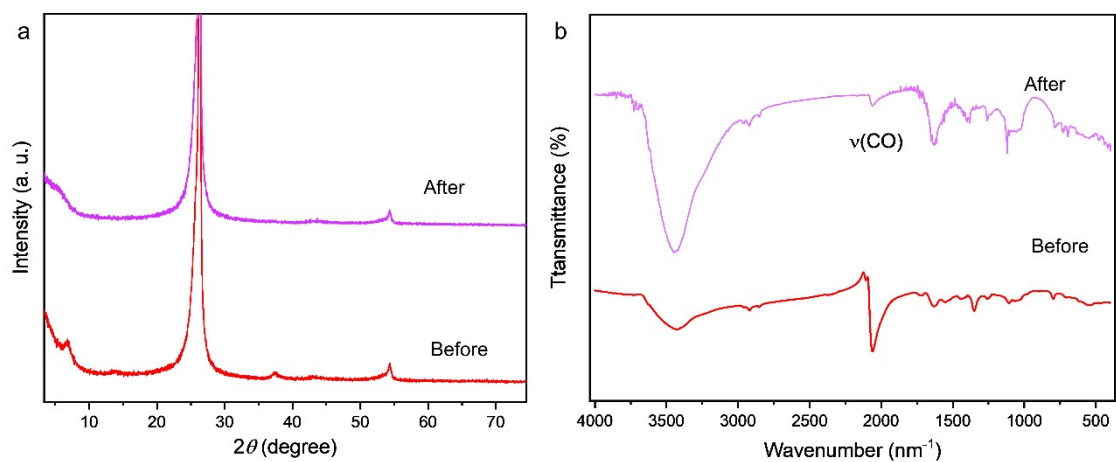


**Fig. S13.** (a) XRD patterns and (b) FTIR spectra of the IrCF-BTC materials before and after electrolysis in 0.1 M  $\text{HClO}_4$  solution.

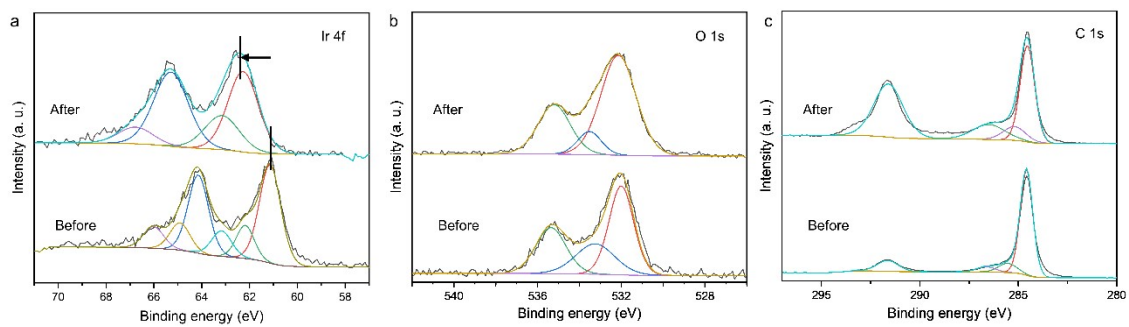


**Fig. S14.** X-ray photoelectron spectroscopy characterization of the IrCF-BTC sample before and after electrolysis. (a) Ir 4f, (b) O 1s, and (c) C 1s high-resolution spectra.

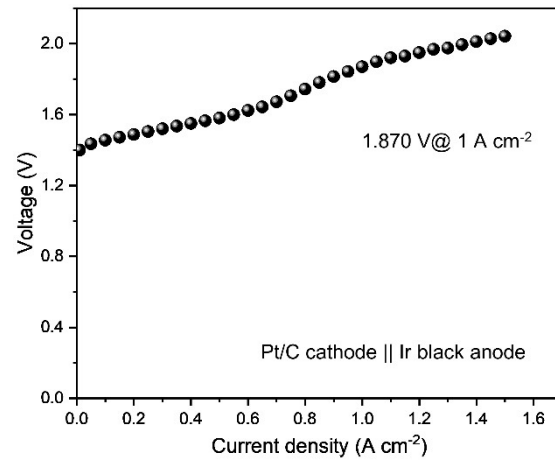


**Fig. S15.** PEM test using Ir black as anode and Pt/C cathode materials.

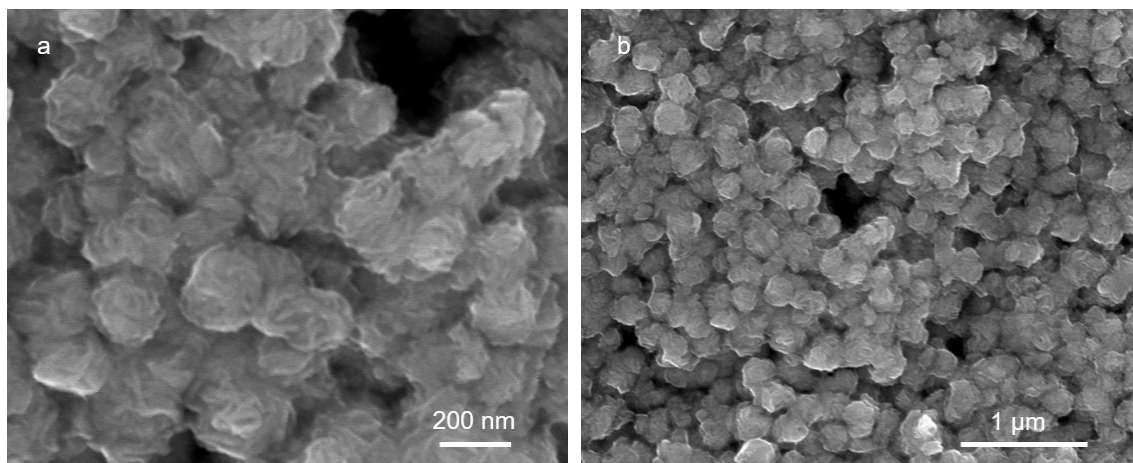


**Fig. S16.** (a, b) SEM images of IrCF-BTC loaded on the MEAs, after testing for more than 100 hours in the PEMWE device with operating current density of  $1.0 \text{ A cm}^{-2}$  under  $80 \text{ }^\circ\text{C}$ .

### **Supporting References:**

S1 G. Kresse, D. Joubert, *Phys. Rev. B*, 1999, 59, 1758-1775.

S2 J. P. Perdew, K. Burke, M. Ernzerhof, *Phys. Rev. Lett.*, 1996, 77, 3865-3868.

S3 G. Stefan, *J. Comput. Chem.*, 2006, 27, 1787-1799.